Soft Matter

Examining platelet adhesion via Stokes flow simulations and microfluidic experiments

Journal:	*Soft Matter*
Manuscript ID:	SM-ART-07-2014-001450.R1
Article Type:	Paper
Date Submitted by the Author:	02-Sep-2014
Complete List of Authors:	Fitzgibbon, Sean; Stanford, Chemical Engineering Cowman, Jonathan; Royal College of Surgeons in Ireland, Molecular and Cellular Therapeutics Shaqfeh, Eric; Stanford University, Chemical Engineering Ricco, Antonio; Stanford University, Department of Electrical Engineering; Dublin City University, Biomedical Diagnostics Institute Kenny, Dermot; Royal College of Surgeons in Ireland, Molecular and Cellular Therapeutics

ARTICLE TYPE www. rsc.org/xxxxxx | XXXXXXXX

Examining platelet adhesion vis Stokes flow simulations and microfluidic experiments

Sean Fitzgibbon,[a] Jonathan Cowman,[b] Antonio J. Ricco,[c] Dermot Kenny,[d] and Eric S. G. Shaqfeh*[e]

Received Xth XXXXXXXXXX 20XX, Accepted Xth XXXXXXXXX 20XX
First published on the web Xth XXXXXXXXXX 200X
DOI: 10.1039/b000000x

While critically important, platelet function at the high shear rates typical of the microcirculation is relatively poorly understood. Using a large scale Stokes flow simulation, Zhao et al. recently showed that RBC-induced velocity fluctuations cause platelets to marginate into the RBC free near-wall region [Zhao *et al., Physics of Fluids*, 2012, **24**, 011902]. We extend their work by investigating the dynamics of platelets in shear after margination. An overall platelet adhesion model is proposed in terms of a continuous time Markov process, and the transition rates are established with numerical simulations involving platelet-wall adhesion. Hydrodynamic drag and Brownian forces are calculated with the boundary element method, while the RBC collisions are incorporated through an autoregressive process. Hookean springs with first order bond kinetics are used to model receptor-ligand bonds formed between the platelet and wall. The simulations are compared with in-vitro microfluidic experiments involving platelet adhesion to Von Willebrand Factor (VWF) coated surfaces.

1 Introduction

1.1 Hemostasis, Red Blood Cells, and Platelet-Protein Interactions

It is well known that platelets play a critical role in hemostasis and thrombosis [1], but the physics behind thrombus formation is still a matter of intense research interest. Recently, it has become apparent that thrombus formation is not solely dependent on platelet adhesion receptors; fluid flow also has an important role in mediating platelet function. For example, Valeri and coworkers [2] reported that, following surgery, lowered platelet concentration has a very small effect on overall bleeding time. In contrast, they noted that a decreased red blood cell (RBC) concentration, or hematocrit (Ht), was strongly correlated with longer bleeding time, i.e. slower coagulation. To explain the nonintuitive dependence of platelet function on hematocrit, Zhao et al. [3] studied platelet margination with large scale numerical simulations of blood flow. They found that the combination of RBC deformability and shear flow drives the RBC center of mass away from vessel walls, creating the well known, RBC-free, Fahreus-Lindqvist (F-L) layer near the wall. Furthermore, frequent collisions of platelets with RBCs in the blood stream core force the platelets to the vessel boundaries, causing elevated local platelet concentrations near the wall. As thrombus nucleation begins at the wall, they suggested that the raised platelet concentration causes the correlation between hematocrit and bleeding time.

Once a platelet is inside the cell free F-L layer, adhesion is mediated by receptor-ligand bonds between the platelet and blood vessel wall. *In vivo*, damaged endothelial cells expose collagen fibers, recruiting Von Willebrand Factor (VWF), a very large glycoprotein, from the blood stream. The wall-bound VWF undergoes a conformational change enabling the capture of glycoprotein 1b (GPIb) [4, 5, 6], a platelet surface receptor (25,000-50,000 copies per platelet [7]). The weak GPIb-VWF bond transiently tethers the platelets and initiates thrombus formation at the site of vascular injury [8]. Under conditions of arterial shear, the GPIb-VWF bond is fast-forming but short-lived, generally lasting for only a few tenths of a second [9]. As multiple bonds break and form, the platelet undergoes a start-stop rolling motion described as saltatory by Shen and coworkers[10]. This transiently adhered state lengthens the platelet contact time with vessel walls, allowing firm adhesion through the platelet surface integrin $\alpha_{IIb}\beta_3$, which binds to VWF [11] or exposed fibrinogen.

[a] *Chemical Engineering, Stanford University, Stanford, CA.*
[b] *Biomedical Diagnostic Institute, Royal College of Surgeons in Ireland, Dublin 2, Ireland*
[c] *Biomedical Diagnostics Institute, Dublin City University, Dublin 9, Ireland*
[d] *Biomedical Diagnostics Institute, Royal College of Surgeons in Ireland, Dublin 2, Ireland. Biomedical Diagnostics Institute, Dublin City University, Dublin 9, Ireland*
[e] *Chemical Engineering, Mechanical Engineering, Institute for Computational and Mathematical Engineering, Stanford University, Stanford, CA. Fax: (650) 723-3764; Tel: (650) 725-3525; E-mail: esgs@stanford.edu*

1.2 Understanding Dynamic Platelet-Surface Interactions

The interplay between shear flow forces and receptor kinetics determines the overall platelet adhesion rate. By analytically solving for a sphere suspended in a Stokesian, wall-bounded shear flow, Goldman, Cox, and Brenner [12] provided the first hydrodynamic drag force theory applicable to platelet dynamics (see [13] for a simpler solution). Thus, early simulations involving particles near walls accounted for hydrodynamic forces by assuming that the particles of interest were hard spheres and appealing to the Goldman-Cox-Brenner theory. While this gives a reasonable approximation for the fluid forces, the corresponding theory for receptor-ligand bonds was not considered until Bell published his seminal work on specific adhesion [14], a theory which he later combined with simple unbound fluid flows [15].

By merging the hydrodynamic forces of Goldman et al. with a Bell-like receptor force, Hammer and Lauffenberger [16] introduced the concept of modeling particle-wall adsorption, and this work had a strong impact on most subsequent models. Cozens-Roberts and coworkers extended the work by acknowledging that specific adhesion events often involve very small numbers of bonds [17]. Thus, they introduced a stochastic element to the receptor dynamics, allowing for explicit bond formation and breaking. Using hard spheres, Hammer and Apte investigated selectin-mediated neutrophil adhesion [18]. Chang et al. [19], Sun et al. [20], and Jadhav et al. [21] all studied leukocyte rolling, using verious analytical and numerical methods to model fluid drag and RBC effects. Blyth and Pozrikidis focused on platelets and the influence of particle shape on hydrodynamic interactions [22].

To date, the most complete model of platelet adhesion, termed "platelet adhesive dynamics," was introduced by Mody and King in 2008 [23]. They treated platelets as rigid ellipsoids and calculated the hydrodynamic drag forces after solving the full Stokes flow equations. Their platelet receptors, Hookean springs with equilibrium lengths, stochastically attached and detached from the vessel wall with first order rate kinetics. Wang, Mody, and King [24] extended this model by incorporating new receptor dynamics and exploring two-platelet collisions. More details and the related literature can be found in Wang and King's review article [25].

In this paper, we explore the initial adhesion of platelets to a VWF-coated surface using a simulation supported by *in vitro* experiments. In section 2 we describe our model. Next, the experiments are introduced along with the closely related numerical simulations. Thereafter, we present our results along with biophysical descriptions of the system. The final section places our results within the framework of our model.

2 Model

Hemostasis and thrombosis are dependent on many factors including RBC concentration, platelet geometry, dozens of ligand-receptor pairs, intra and intercellular signaling cascades, and platelet collisions to name a few. It is impractical to account for every aspect, so we build a simplified system that captures the dominant physics. At its core, the model is composed of a four state, continuous time Markov process, as show in Figure 1. Over time platelets transition between these four states as a result of hydrodynamic collisions and ligand-receptor bond formation. First order transition rates are assumed, with rate constants r_{ij} (rate constant from state i to state j).

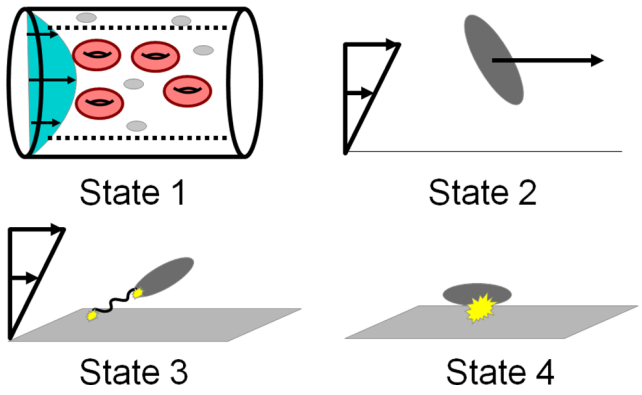

Fig. 1 State Diagram

Platelets in state 1 are found in the blood vessel core, which is the RBC-full region surrounded by the F-L layer. State 2 is composed of platelets inside the F-L layer which have not yet attached to the wall. Because this layer is very thin compared to the core [26], curvature effects are neglected. Thus, in state 2 platelets are modeled as particles in wall-bounded shear flow. State 3 consists of transiently adherent platelets. In this case, there exist one or more short-lived VWF-GPIb bonds which connect each platelet to the wall. In the final state (4), platelets are firmly adhered to the surface through integrin $\alpha_{IIb}\beta_3$. We assume that the rate of platelet-plug formation is largely controlled by the initial platelet adhesion rate to the wall, which allows the model to be restricted to single platelet dynamics.

The model is completed by establishing the transition rates (r_{ij}) between the distinct states along with the relationship between r_{ij} and the various physical parameters. Fortunately, a number of these rates are negligible. The short ranges of receptor-ligand interactions ($O(100nm)$) indicate that platelet-wall adhesion (and detachment) can only occur for platelets inside the F-L layer ($O(1\mu m)$). Thus, direct transitions between the vessel core, state 1, and the adherent states, 3 and

4, are forbidden, i.e. $r_{13} = r_{14} = r_{31} = r_{41} = 0$. Furthermore, the $\alpha_{IIb}\beta_3$ bond which mediates firm adhesion, is irreversible [27, 28] over the experimental time scale, so platelets cannot return to any previous state following firm adhesion, i.e. $r_{42} = r_{43} = 0$. Finally, as is shown in Figure 2, the $\alpha_{IIb}\beta_3$-VWF bond forms approximately 350 times slower than the GPIb-VWF bond. Thus, r_{24}, or the transition rate for platelets which firmly adhere directly from the near-wall state, can be safely neglected. Five finite rate constants remain: r_{12}, r_{21}, r_{23}, r_{32}, and r_{34}. Once these constants are determined, the platelet fractions in each state are determined with the following equations.

$$\begin{aligned}
\frac{d[\text{State 1}]}{dt} &= -r_{12}[\text{State 1}] + r_{21}[\text{State 2}] \\
\frac{d[\text{State 2}]}{dt} &= r_{12}[\text{State 1}] - r_{21}[\text{State 2}] - r_{23}[\text{State 2}] + r_{32}[\text{State 3}] \\
\frac{d[\text{State 3}]}{dt} &= r_{23}[\text{State 2}] - r_{32}[\text{State 3}] - r_{34}[\text{State 3}] \\
\frac{d[\text{State 4}]}{dt} &= r_{34}[\text{State 3}]
\end{aligned} \tag{1}$$

[State i] indicates the fraction of platelets in state i. The rates r_{ij} are determined by combining large scale RBC simulations previously described in [3], microfluidic experiments, and platelet adhesion simulations.

Table 1 Parameter estimates

Parameter	Estimate
shear rate	1,500 s^{-1}
platelet Jeffery orbit timescale	10 ms
experiment camera exposure time	33 ms
platelet radius	1 μm
near wall suspended platelet velocity	1 mm / s
transiently adhered platelet rolling velocity	10 μm / s
Adherent platelet hydrodynamic drag force	40 pN
Fahreus-Lindqvist layer viscosity	0.0015 Pa s
Blood density	1060 kg/m^3
Reynolds number	0.0007
Peclet number	23,000

To place this work in an overall fluid mechanics context, we report the physically relevant length and time scales of our simulations and experiments in Table 1. The Reynold number is very small (below 0.001) everywhere, so Stokes flow provides a good theory for hydrodynamic forces. With a Peclet number of over 10^4, Brownian motion has a relatively weak effect, so in whole blood, diffusion is dominated by RBC collisions [3]. Furthermore, platelets occupy a tiny fraction of blood in comparison to RBCs, so we expect that platelet-platelet collisions have a negligible effect on the system dynamics. As platelets are much less flexible than RBCs [3], platelets are modeled as rigid oblate ellipsoids with aspect ratio 3:1. No obvious deformation was visible in our experiments, further supporting the rigidity assumption, and the 3:1 ratio falls within the physical range reported by Moskalensky[29].

Zhao et al. reported shear-induced dispersion effects which are an order of magnitude greater than simple Brownian motion in platelets [3], so our near wall simulations must include RBC collisions. While they also calculated diffusion constants for this process, the autocorrelation times were comparable to the Jeffery orbit flow time scale (10 ms). Thus, RBC-platelet collisions cannot be modeled as delta correlated, and an autoregressive process (diffusion with memory) is used. Platelets interact with many RBC's over the course of a single Jeffery orbit, so we incorporate platelet-RBC interactions with a mean field theory. There are six rigid body modes that can be excited by a collision with three translations and three rotations. The natural question arises: are all six modes important? Extra translations in the flow direction are negligible because these fluctuations are very small with respect to the shear flow. By symmetry, translations in the vorticity direction do not change the system and can also be neglected. Extra collisional rotations occur on a 10ms time scale, which is much smaller than the bond formation time scale (200 ms). During a single bond formation event, the platelet has plenty of time to "explore" the rotational states without adding in extra collisional rotation. We conclude that the most important effect of platelet-RBC collisions is the extra translational motion in the wall-normal direction, and the autocorrelation time is included using an autoregressive process with appropriate parameters extracted from Zhao et al.'s simulations.

There are two receptor-ligand bonds that are important for the overall platelet adsorption process. The first is the VWF-GPIb bond, which is responsible for the (initial) transient or rolling adhesion which precedes "persistent" adhesion. We introduce four parameters to define the VWF-GPIb bond dynamics. The attachment and detachment reaction rate constants are $k_{\text{on}}^{\text{weak}}$ and $k_{\text{off}}^{\text{weak}}$ respectively, the bond formation length scale is L, and the spring stiffness is represented with k. Doggett et al. [30], among others, have established that the VWF-GPIb bond releases with first order kinetics, with $k_{\text{off}}^{\text{weak}} \sim 5s^{-1}$. Similar to Mody and King [23], we assume a first order forward reaction, and $k_{\text{on}}^{\text{weak}}$ is fit to experimental data. This necessarily involves the introduction of a length scale over which the platelet can interact with the surface. GPIb is a small receptor, while VWF is very large relative to GPIb, so the length scale, L, depends on the size of VWF. VWF self-aggregates [31], and AFM measurements have shown that it grows to a size of several hundred nanometers [32]. Thus, we have chosen an average value of $L \sim 200nm$ for our simulations.

To model first order kinetics within the simulations, the process is separated into two steps, bond release and bond formation. At the beginning of each time step, there are N^{weak} weak bonds (GPIb) and N^{strong} strong bonds ($\alpha_{IIb}\beta_3$). The strong bonds are considered irreversible and do not release. Each weak bond is a candidate for release, with rate constant $k_{\text{off}}^{\text{weak}}$. The probability of a bond remaining attached after a certain period of time is calculated with the following linear ordinary differential equation. The initial condition says that the bond exists at the beginning of the time step.

$$\frac{dP(\text{attached})}{dt} = -k_{\text{off}}^{\text{weak}} P(\text{attached}) \qquad (2)$$
$$P(\text{attached at } t = 0) = 1$$

The solution is an exponential, which can be used to calculate the probability of bond breaking by the end of the time step.

$$P(\text{attached at } t = \Delta t | \text{attached at } t = 0) = e^{-k_{\text{off}}^{\text{weak}} \Delta t} \qquad (3)$$
$$P(\text{bond breaking in } \Delta t) = 1 - e^{-k_{\text{off}}^{\text{weak}} \Delta t}$$

For each of the N^{weak} weak bonds present at the beginning of a time step, a uniform U(0,1) random number is drawn. If this random number is below the probability of breaking, the bond is removed from the simulation.

After bond release, bond formation is considered. Since, we are assuming first order rate kinetics, the average number of bonds formed in a very small time period is proportional to both the rate constant and the surface area exposed by the platelet. Thus, the average bond formation number for a small time, Δt, must be $k_{\text{off}}^{\text{weak}} A(L)\Delta t$ (or $k_{\text{on}}^{\text{strong}} A(L)\Delta t$ for strong bonds), where $A(L)$ is the surface area of the platelet within a distance L of the wall. By assuming that $A(L)$ is constant over the time step, we arrive at a Poisson distribution for bond formation.

$$P(n \text{ weak bonds formed in } \Delta t) = \frac{\left(k_{\text{on}}^{\text{weak}} A \Delta t\right)^n}{n!} e^{-k_{\text{on}}^{\text{weak}} A \Delta t} \qquad (4)$$

$$P(n \text{ strong bonds formed in } \Delta t) = \frac{\left(k_{\text{on}}^{\text{strong}} A \Delta t\right)^n}{n!} e^{-k_{\text{on}}^{\text{strong}} A \Delta t}$$

At each time step, two random variables are drawn from these distributions, corresponding to the number of weak and strong bond formation events in that time step. The newly formed bonds are placed uniformly over the exposed platelet surface area.

Mody and King estimate the stiffness of the GPI-VWF bond at 10pN/nm [23], but our receptor-ligand bonds are modeled without an equilibrium length. Using 10pN/nm would result in an unreasonably short bond length in our simulations. An estimate of the hydrodynamic drag on a platelet under conditions of arterial shear can be obtained using Stokes law, giving a value of O(40 pN) for a shear rate of 1500 s^{-1} (Figure 17 validates this estimate). With a 100 pN/μm spring constant, the equilibrium length of a single bond system would be only 4nm, much smaller than the size of VWF. To simplify the system (which includes removing the zero-force bonds length), we must choose a significantly lower spring stiffness to allow for VWF sized bonds. Shiozaki et al. estimated a bond stiffness of $k = 100\text{pN}/\mu\text{m}$, which we use in our simulations.

Similar to the weak bond involving GPIb, four parameters are used for the strong bonds (mediated by integrin $\alpha_{IIb}\beta_3$). Persistent adhesion is very stable compared to transient adhesion, with $k_{\text{off}}^{\text{strong}} \sim 10^{-2} s^{-1}$ [33]. This rate constant leads to an effective bond lifetime of 100 seconds, which is much longer than the experimental time scale of 15 seconds. Thus, strong detachment is effectively forbidden, and the rate constant is approximated as $k_{\text{off}}^{\text{strong}} = 0$. Like $k_{\text{on}}^{\text{weak}}$, $k_{\text{on}}^{\text{strong}}$ is fit to experimental data, and the approximation $L_{\text{strong}} = L_{\text{weak}} = L$ is used because both bonds form through the large glycoprotein, VWF. This just leaves the value for spring (bond) stiffness, which is chosen as equivalent to the weak spring case, again because both bonds involve VWF. We note that our simulations are completed after firm adhesion, so the accurate evaluation of strong spring stiffness is not critical. The receptor model and parameters are summarized in Figure 2.

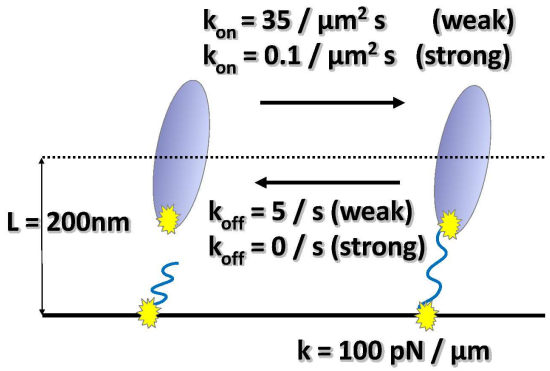

Fig. 2 Receptor Parameters

3 Methods

3.1 Experimental Methods

We have previously described a microfluid flow-based system and unique platelet tracking algorithm to characterize platelet interactions with immobilized human VWF in a custom-designed microfluidic parallel-plate flow chamber under conditions of arterial shear (1500 s^{-1}) [34]. This system and its applications are summarized briefly below.

3.1.1 Blood Collection. Blood was obtained from healthy volunteers recruited within the Royal College of Surgeons in Ireland (RCSI). All healthy volunteers were free from any medication known to affect platelet function within the previous 10 days. Prior to blood draw all volunteers were required to sign written informed consent. Blood was drawn through a 19-gauge butterfly needle into a polypropylene syringe (Becton Dickinson, Oxford, UK) containing a 3.2% solution of the anti-coagulant, trisodium citrate dihydrate.

3.1.2 Microfluidic Parallel Plate Flow and Preparation. To minimize blood volume requirements and ensure uniform laminar flow shear rate we have adapted a customized microfluidic parallel plate flow device previously described by Kent et al [34]. A schematic of the device is shown in Figure 3. The microfluidic devices are comprised of three parts including 25 x 55mm polymethylmethacrylate (PMMA) top plate containing inbuilt 1/16-mm polypropylene inlet and outlet connecters (Ensinger Plastics, UK), an acrylic adhesive gasket (Adhesives Research, Limerick, Ireland) defining/containing the microfluidic channel (2mm wide, 50μm in high, 30mm long) and a 24x55 mm, 160-190 μm thick, glass microscope coverslip (Bio-World, Dublin, OH, USA). The surface of the coverslip is spotted with fluorescently labelled bovine serum albumin (BSA) in select locations to assist with microscope focusing prior to platelet adhesion.

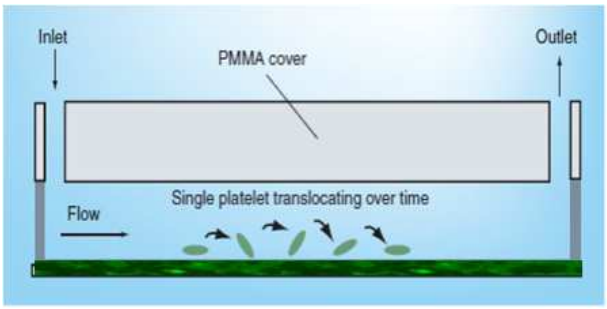

Fig. 3 Cross section of microfluidic device. The bottom surface is coated with VWF.

On the coverslip surface of the parallel-plate flow device channel purified human VWF (courtesy of Robert Montgomery, Blood Research Institute, Milwaukee, WI, USA) is passively immobilized by adsorption from a 100 μg/mL solution in phosphate buffered saline (PBS 10 mM phosphate buffer, 2.7 mM potassium chloride, and 137 mM sodium chloride, pH 7.4) for 12 h. The surface is then washed with PBS and blocked with 1% (unlabeled) BSA for 1 h at room temperature, followed by a final rinsing step in PBS prior to perfusion of whole blood.

3.1.3 Whole Blood Perfusion and Image Acquisition. Blood samples are incubated with a lipophilic dye, DiOC6 (1 μM; Invitrogen, Carlsbad, CA, USA) at 37ºC for 10 min for visualization of platelets in a background of flowing whole blood. Blood is drawn through bio-compatible platinum-cured silicone tubing (Nalgene, 1.6mm internal diameter, Thermo Fisher Scientific, Denmark) into the flow channel of the assembled microfluidic device. A Nemesys syringe pump (model NEM-8001-02-C, Cetoni, Germany) is used to draw the blood through the device at a controlled flow rate of 75μL/min, resulting in a fluid shear rate of 1,500s^{-1}, in the physiologically relevant arterial range. A shear stress of 6 Pa occurs at the bottom wall surface of the chamber (i.e. the VWF-coated coverslip), where interacting platelets are imaged. Flow chambers are mounted on an inverted microscope (Zeiss Axiovert-200 epi-flouresence) with an Osram 103-W mercury light source and a fluorescein isothiocyanate (FITC) filter set (excitation 490/20x, emission 528/38m, Chroma Technology Corp, Vermont, USA) Images were captured using a cooled (-80ºC) digital EM-CCD camera (iXON3 885 EM-CCD sensor, Andor Technology, Belfast, N. Ireland), with a viewing region of 512 x 512 pixels at 63x magnification. The microscope output is processed using MetaMorph software (version 7.7, Molecular Devices Ltd., UK). Images are recorded beginning 3-5s after initial platelet interactions with the VWF surface for a period of 500 frames at 30 frames per second (FPS), or 16.7s. A sample frame is shown in Figure 4.

Initial platelet interactions with the surface include reversible tethering through weak bonds that are readily released. This causes the platelets to enter a rolling state: as weak bonds with the VWF surface are broken and new bonds form; a stop start motion known as translocation results. This process is key in iniating thrombosis by attaching platelets to the surface: translocation allows engagement and activation of further receptors resulting eventually in stable (persistent) platelet adhesion [11, 35].

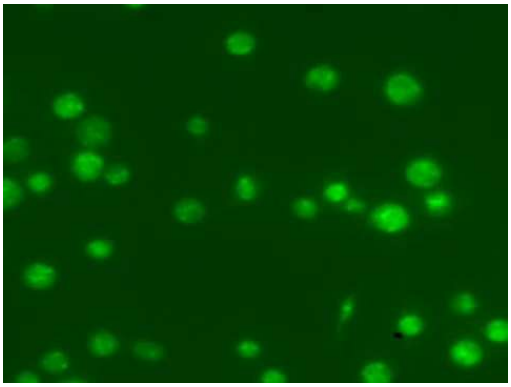

Fig. 4 rolling platelets on VWF surface

3.1.4 Image Analysis. Initial platelet interactions (tethering, rolling and translocation) with VWF surfaces were analyzed via a modified version of a customized platelet tracking algorithm created in MatLab (version R2008b, MathWorks, UK). Platelets labeled with a fluorescent dye are identified in each of the 500 frames of a flow run. An auto-threshold method is used to reliably detect and record the x,y centroid position and to define the approximate size of each platelet present in a given frame (against a time-varying background). From one frame to the next the platelet is tracked and its trajectory constructed. A weighted distance matrix is applied between the platelet's current position and all platelets in the subsequent frame. This track definition process gives preference to platelet movement in the direction of flow at reasonable speeds over cross-stream or up-stream movement. Each of the platelet trajectories is extended by assigning it to the appropriate platelet in the next frame. Two or more platelets merging into one object or, conversely, one splitting into two is detected by examining platelet area. Finally a list of trajectories corresponding to position and movement from frame to frame is generated for each platelet in the image sequence. Overall, this algorithm is similar to the method described by Lincoln *et. al.* [34], but it contains significant enhancements that account for the tracks of partially overlapping platelets merging and splitting.

3.1.5 Measured Parameters. From the collection of platelet tracks for a given 500-frame flow run, two parameters were collected: the fraction of platelets which firmly adhered, and the translocation distance. A platelet was classified as bound if it was still attached to the surface on the last frame. Platelets which disappeared from the field of view (reentered the flow), were classified as released. The translocation distance was calculated as the difference in platelet position between the first and last frame, measured in the flow direction.

3.2 Numerical Methods

3.2.1 Surface Mesh. Platelets are treated as 3:1 oblate ellipsoids, and the surface is meshed with an irregular triangulation based on the work of Boissonnat [36]. In this algorithm, the surface mesh is extracted from an underlying volume mesh built with a Delaunay triangulation. In memory, the mesh connectivity is represented with Mucke and Edelsbrunner's triangle edge structure [37], while the implicit surface is defined by an oracle function. The input to the oracle is a line segment, and the output is the set of segment-surface intersection points. Triangles which are too large or skinny (as defined by a mesh quality function) are refined by adding new vertices inside the offending triangles. Finally, for robustness geometric predicates must be calculated very accurately for robustness, so we use variants of the adaptive exact-precision predicates originally introduced by Shewchuk [38].

3.2.2 Boundary Element Equations. The Stokes flow equations are solved with a single layer formulation of the boundary integral equations (5), using Blake's wall bounded Stokeslet for the Green's function. Although this leads to a Fredholm equation of the first kind, we did not observe any numerical problems with the test cases or solutions, consistent with the observations of Youngren and Acrivos[39]. The traction is discretized with piecewise constant shape functions, labeled as ϕ_i^I, and Galerkin's method is used to discretize the equations while guaranteeing a symmetric stiffness matrix. The full set of equations is shown in equation (6). To invert the symmetric stiffness matrix, MINRES is applied, and hydrodynamic forces and torques are calculated by integrating the surface traction, $\mathbf{f}(\mathbf{x})$. For a given particle configuration, the Stokes flow solver output is the resistance tensor, $\mathbf{R}$, and the hydrodynamic drag force caused by infinite shear flow, $\mathbf{F}^{\infty}$.

$$u_j(\mathbf{x}_0) = -\frac{1}{8\pi}\int G_{ij}(\mathbf{x},\mathbf{x}_0) f_i(\mathbf{x}) dS_{\mathbf{x}} \tag{5}$$

$$\sum_I \left(\int\int \phi_i^I(\mathbf{x}) G_{ij}(\mathbf{x},\mathbf{x}_0) \phi_j^J(\mathbf{x}_0) d\mathbf{x} d\mathbf{x}_0 \right) a^I = -8\pi \int u_j(\mathbf{x}_0)\phi_j^J(\mathbf{x}_0) d\mathbf{x}_0 \tag{6}$$

The subscripts i and j are the vector components of ϕ^I, while I and J identify the element (three elements per triangle corresponding to the x, y, and z direction). We tested our solution method on a sphere near a wall, for which analytic solutions are available [12]. The error in the resistance tensor was less than 3% until the sphere approached within half an element size (average triangle circumradius) of the surface.

3.2.3 Particle Motion. Throughout this section, $\mathbf{F}$, $\mathbf{U}$, and $\mathbf{x}$ represent generalized forces, velocities, and displacements, respectively. Each has six components. The first three components represent the standard force, velocity, or displacement, while the last three represent torque, angular velocity, or angular displacement. Our Euler time stepping follows the theory of Banchio and Brady [40]. We begin by assuming Stokes flow and sum the particle forces.

$$\mathbf{F}^{\text{drag}} + \mathbf{F}^{\infty} + \mathbf{F}^{\text{R}} + \mathbf{F}^{\text{drift}} + \mathbf{F}^{\text{B}} = 0 \tag{7}$$

$\mathbf{F}^{\text{drag}}$ is the hydrodynamic drag force created by the particle motion in a quiescent fluid, $\mathbf{F}^{\infty}$ is the hydrodynamic drag from the infinite shear flow, the Brownian force is $\mathbf{F}^{\text{B}}$, and the drift force associated with a varying resistance tensor is $\mathbf{F}^{\text{drift}}$. $\mathbf{F}^{\text{R}}$ represents the receptor force, which is the only force calculated independently of the Stokes flow solver. The generalized receptor force can be decomposed into its constituent force and torque ($\mathbf{F}^R = \left[\mathbf{f}^{\text{R}}, \tau^{\text{R}}\right]^T$).

$$\mathbf{f}^{\mathrm{R}} = \sum_{n \in \text{bound receptors}} k_n \left(\mathbf{x}_n^{\text{head}} - \mathbf{x}_n^{\text{tail}} \right) \quad (8)$$

$$\tau^{\mathrm{R}} = \sum_{n \in \text{bound receptors}} k_n \left(\mathbf{x}_n^{\text{tail}} - \mathbf{x}^{\mathrm{CoM}} \right) \times \left(\mathbf{x}_n^{\text{head}} - \mathbf{x}_n^{\text{tail}} \right) \quad (9)$$

In these equations, head and tail refer to the receptor attachment points on the wall and platelet, respectively. $\mathbf{x}^{\mathrm{CoM}}$ is the center of mass of the platelet, and the k_n's represent the spring stiffness for each receptor. $\mathbf{x}_n^{\text{tail}}$ is a 3-tuple describing the tail position of spring n in 3-space. The torque is described with vector cross products.

The rest of the forces are dependent on the Stokes solver described above. Recall that $\mathbf{R}$ and $\mathbf{F}^{\infty}$ are outputs from the Stokes solver. The hydrodynamic force $\mathbf{F}^{\text{drag}}$ is used to solve for the particle displacement, $\Delta\mathbf{x}$, at each time step.

$$\mathbf{F}^{\text{drag}} = -\mathbf{R}\mathbf{U} = -\mathbf{R}\Delta\mathbf{x}/\Delta t \quad (10)$$

$$\Delta\mathbf{x} = \mathbf{R}^{-1}\left(\mathbf{F}^{\infty} + \mathbf{F}^{\mathrm{R}}\right)\Delta t + \mathbf{R}^{-1}\left(\mathbf{F}^{\mathrm{B}} + \mathbf{F}^{\text{drift}}\right)\Delta t$$

The two remaining terms are the Brownian force, $\mathbf{F}^{B}$, and the drift force, $\mathbf{F}^{\text{drift}}$. The Brownian force is defined with the square root of the resistance matrix (calculated with the Cholesky decomposotion $\mathbf{R}^{-1} = \mathbf{A}\mathbf{A}^{T}$).

$$\mathbf{R}^{-1}\mathbf{F}^{\mathrm{B}}\Delta t = \sqrt{2kT\Delta t}\mathbf{A}\mathbf{N}(t) \quad (11)$$

k and T are the Boltzmann constant and absolute temperature, and $\mathbf{N}$ is a set of six Gaussian random variables (zero mean and unit standard deviation). The final term is the drift term, which depends on the Brownian force. We begin by assuming that the only forces are $\mathbf{F}^{\mathrm{B}}$ and $\mathbf{F}^{\text{drag}}$. The system is then time stepped forward into a temporary new configuration, using a small step $n = 0.01\Delta t$. The Stokes flow solver is called at this new configuration to form a temporary resistance matrix $\mathbf{R}'$. With $\mathbf{R}'$ in hand, $\mathbf{U}^{\text{drift}}$ is calculated and the system is returned to the original configuration (ready to move forward a full time step). $\mathbf{U}^{\text{drift}}$ is then defined as:

$$\mathbf{U}^{\text{drift}} = \mathbf{R}^{-1}\mathbf{F}^{\text{drift}} = \frac{n}{2}\left(\mathbf{R}'^{-1}\mathbf{F}^{\mathrm{B}} - \mathbf{R}\mathbf{F}^{\mathrm{B}}\right) \quad (12)$$

For a more complete discussion of rigid body Brownian dynamics simulations, the reader is encouraged to consult Banchio and Brady [40] and its references.

3.2.4 RBC collisions. As discussed in section 2, RBC-platelet collisions are modeled with an autoregressive (AR) process by fitting the regression coefficients to Zhao et al.'s autocorrelation times [3]. Five autocorrelation values provide a reasonable estimate of the entire range of autocorrelations, and the Yule-Walker equations are used to convert these coefficients into the standard AR coefficients ϕ_i [41]. The RBC-platelet collision term takes the form of an extra velocity added at the end of each time step, as shown in equation (13).

$$v_i^{extra} = \phi_1 v_{i-1}^{extra} + \phi_2 v_{i-2}^{extra} + \phi_3 v_{i-3}^{extra} + \phi_4 v_{i-4}^{extra} + \phi_5 v_{i-5}^{extra} + N_i \quad (13)$$

In this equation, v_i^{extra} is the velocity addition for the current time step, while past timestep values are recorded in v_{i-1}^{extra} etc. N_i is a Gaussian random variable with variance selected by combining the AR coefficients, the zero lag Yule Walker equation, and the velocity root mean square reported in Zhao et al.[3]

4 Results

4.1 Fahreus-Lindqvist Diffusion Timescale

In the first simulation set, we investigate the effect of RBC collisions on the diffusion time scale inside the F-L layer. Platelets enter state 1 at the top of the F-L layer, and must move to the bottom of the layer (close to the wall) before adhering. The time reversibility of Stokes flow along with the rigidity of platelets means that shear flow alone does not drive platelets to the wall, so other physical mechanisms control the rate of transition through the F-L layer. The only two possibilities are thermal diffusion and RBC collisions.

To quantify the F-L crossing time, a platelet is positioned at the top of the F-L layer at time $t = 0$. The simulation is evolved forward in time until the platelet approaches within a distance L of the wall, and the total time is recorded. L is the distance over which weak bonds form, so the simulation time gives a good estimate of the diffusion time scale.

Figure 5 shows the crossing time results for $Ht = 0.1$. Based on the work of Zhao et al. [3], the F-L layer width is 4.2 microns. By including RBC collisions, the mean time to cross the F-L layer is reduced from 37s to 6s, showing that RBC collisions are the main physical mechanism for crossing the F-L layer. For $Ht = 0.2$, a similar reduction in diffusion time is seen in Figure 6. In this case, the F-L layer width is 2.8 microns, and the crossing time reduces from 31s to 2s when blood fluctuations are incorporated.

To establish an accurate rate constant for a platelet moving from the cell-free layer back into the blood vessel core (r_{21}), a more complete description of RBC's, perhaps involving layering, would need to be considered. In our large scale simulations, we have not seen any platelets reenter the core region (State 1) after entering the F-L layer (State 2). As our large scale simulations do not include Brownian fluctuations, we surmise that thermal diffusion must play a large role in establishing (r_{21}). From the results of this subsection, thermal motion is significantly slower than shear induced dispersion.

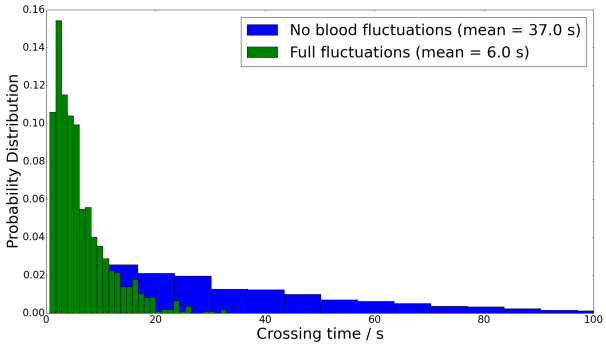

Fig. 5 Time to cross the cell free layer with and without RBC collisions (Ht = 0.1).

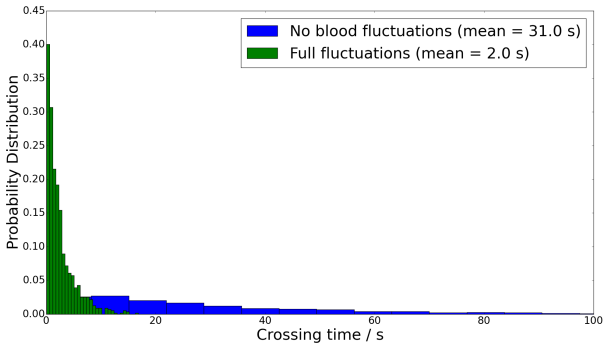

Fig. 6 Time to cross the Cell free layer with and without RBC collisions (Ht = 0.2).

Therefore, we expect that r_{21} is small when compared to r_{12}, and $r_{21} \approx 0$ is a reasonable approximation.

4.2 Fahreus-Lindqvist Reaction Timescale

There are two steps in any adsorption reaction. First, the species diffuses to the wall, and then it reacts with the wall. The previous simulation established the diffusion time scale, and now we investigate the reaction time scale, beginning with platelets inside the F-L layer. These simulations are essentially the calculation of diffusive Jeffery orbits near a wall. For a fluid mechanical study of these orbits, the reader is encouraged to consult the work of Pozrikidis [42]. Here, we focus on the average bond formation rate associated with the Jeffery orbits.

Large scale simulations, as described in Zhao et al.[3], were used to predict the center of mass distributions for platelets in the F-L layer. The results are shown in Figure 7. The distributions are cut off at the edge of the F-L layer, and as expected, the platelets are shifted closer to the wall for $Ht = 0.2$.

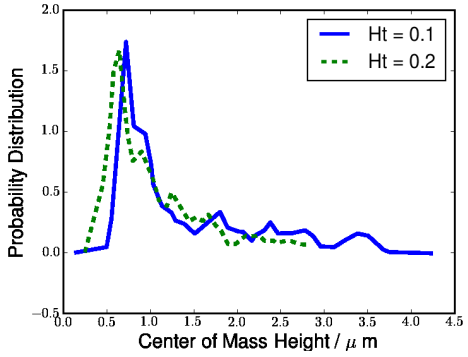

Fig. 7 Platelet center of mass distributions in the F-L layer

To initialize the reaction simulation, the platelet height is sampled from the distributions in Figure 7. The orientation is then chosen from a uniform distribution. The system is evolved forward for several tumbling periods, and the area exposed to the wall is recorded as a function of time. The exposed area fluctuates with time as the platelet tumbles, so the results (Figure 8) are time averaged. The exposed area is a function of the shear flow and the parameter L, but as a consequence of Stokes flow linearity, the dependence on shear flow drops out during time averaging. Thus, the average exposure depends solely on the bond formation length, L. To form the rate constant for transition between states 2 and 3, r_{23}, the average exposed area is multiplied by $k_{\text{on}}^{\text{weak}}$. For $k_{\text{on}}^{\text{weak}} = 35/(\mu m^2 s)$ and $L = 0.2\mu m$, the computed rate constants are $r_{23} = 0.07 s^{-1}$ and $r_{23} = 0.4 s^{-1}$ for $Ht = 0.1$, and $Ht = 0.2$ respectively.

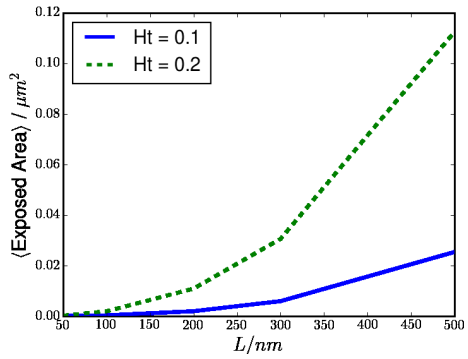

Fig. 8 Average area exposed to surface by a near wall platelet

4.3 Transiently adhered state

The remaining simulations capture the dynamics of a platelet in state 3 (transient adhesion), where direct comparison with

experiment is possible. A platelet enters state 3 with a single GPIb-VWF bond, so each simulation begins with a platelet transiently adhered to the wall through a single GPIb-VWF (weak) bond. The platelet orientation is chosen from a uniform random orientation, and the initial bond is placed at the two points of closest approach betweeen the platelet and wall. A sample initial configuration is presented in Figure 9. In the

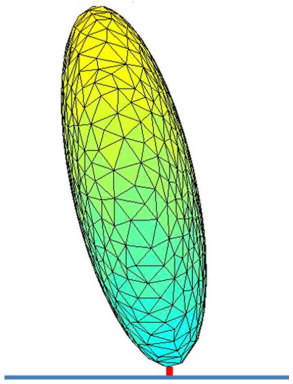

Fig. 9 An initial configuration for transient adhesion simulations

initial configuration, the starting bond is unstressed, so there is an initial transient in which the platelet finds the equilibrium between the hydrodynamic drag force and the ligand receptor bond. For a shear rate of $1500s^{-1}$, the transient occurs in well under 33 ms, which is the frame period of our camera. Since our current setup cannot capture the transient, we remove the first 33 ms from subsequent data analyses.

After the initial transient, platelets undergo a start and stop motion as described in the experimental section. The simulation shows that platelets mostly remain stationary, with small periods (10ms) of quick movement as the trailing bond breaks and a new balance is found between the flow and extant bonds. There are two possible "final states" in our simulations, bound or released. If the platelet forms a strong bond with the surface, or is attached at the end of the simulation (same length of time as in experiment), the platelet is considered bound (entry into state 4). To enter the released state (state 2), the platelet must release all bonds from the surface, reentering the flow.

During the simulation, the platelet trajectory along the surface is recorded. Similarly, platelet trajectories are directly observed in the experiment. Sample tracks, showing qualitative agreement between simulation and experiment, are shown in Figure 10.

For a quantitative comparison with experiment, two quantities are compared. First, the platelet trajectory length in the flow direction is measured in the simulation and the experiment, with the comparison shown in Figure 11. The same results are reproduced in semilog form (Figure 12), showing that in both cases, the distributions are exponential in nature.

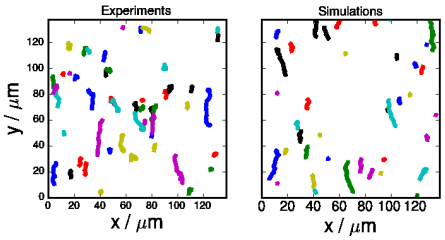

Fig. 10 Paths followed by platelets as a function of time. Each continguous "worm track" represents the time evolving position of one platelet as it translocates in the direction of blood flow (negative y direction).

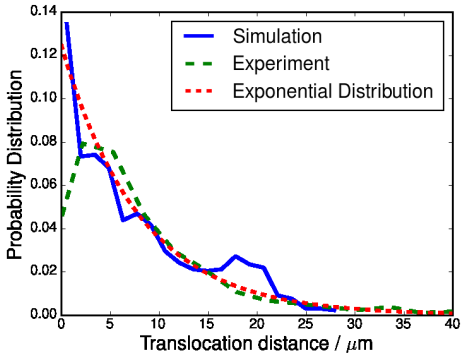

Fig. 11 Trajectory length distributions. The curve is an exponential distribution with mean $8\mu m$.

The second measured quantity is the fraction of bound platelets. k_{on}^{weak} and k_{on}^{strong} were established by fitting both the average translocation distance (8 μm) and the total binding fraction (0.85). The variation of binding fraction with the two forward reaction rate constants is shown in Figures 13 and 14.

After establishing the unknown parameters (the bond formation rates), the model of state 3 is closed with one more simple observable: how quickly does a transiently adherent platelet reenter the flow or firmly adhere? The simulation results are shown in Figure 15, separated into both firmly adhering and transiently adhering subpopulations. In the firmly adhering case, the platelet takes an average of 6 seconds to adhere, while the transient platelets release in 5 seconds on average. Note that a large number of platelets are considered bound at 16s, which corresponds to the end of the simulation (the simulation time was matched to the experimental time). Furthermore, firm adhesion time cannot be measured experi-

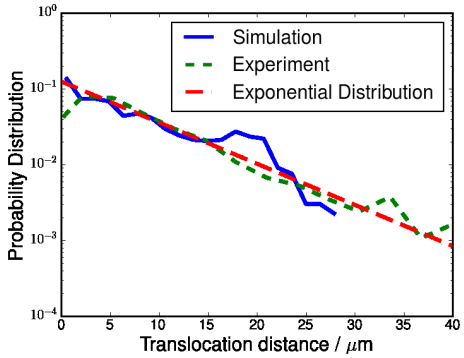

Fig. 12 The trajectory length distributions are exponential in nature. The line is an exponential distribution with mean $8\mu m$.

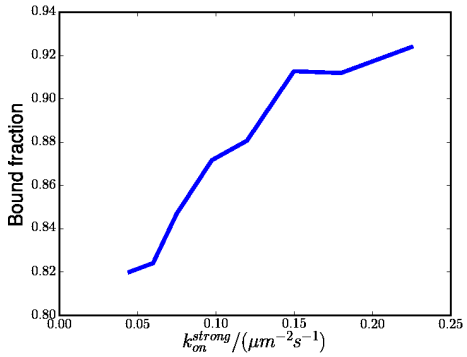

Fig. 14 The variation in binding fraction with the strong forward reaction rate.

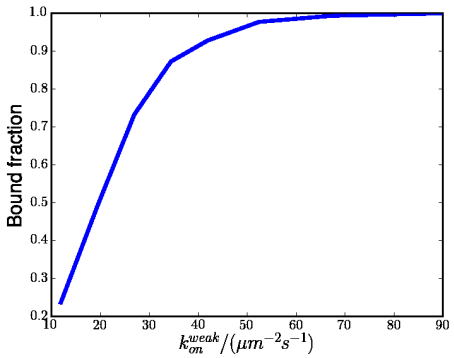

Fig. 13 The variation in binding fraction with the weak forward reaction rate.

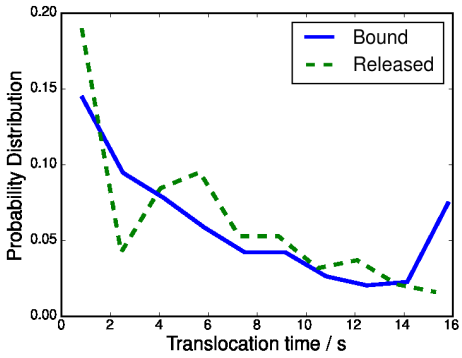

Fig. 15 The time for a platelet to reenter the flow separated into bound and released subpopulations. The increase in firm platelet adhesion at 16s is a result of the finite simulation time (same time period as in the experiment). The released data is noisier, as only 15% of platelets released, leaving a smaller sample size.

mentally, as the individual platelet bonds are not visible.

4.4 Transiently adhered state: shear effects

Repeating the simulation from the previous subsection, we investigate the effects of varying shear rate, $\dot{\gamma}$, which is mainly responsible for a hydrodynamic drag force in the flow direction. Wu et al. [43] found that for shear rates of 300-2600s^{-1} the VWF-GPIb and $\alpha_{IIb}\beta_3$ interactions were critical in thrombus formation on collagen, so we investigate a similar range of shear rates (500-4000s^{-1}). As can be seen in Figure 16, the platelet translocation distances are a weak linear function of shear rate. The translocation distance only increases by a factor of 3 as the shear rate rises from 500s^{-1} to 4000s^{-1}.

To understand the linear dependence of translocation distance on shear rate, we focus on the drag force in the flow direction. In Stokes flow without bond formation, $\dot{\gamma}$ is expected to be linearly related to the drag force, which is realized in Figure 17. Furthermore, Figure 17 shows that the drag force closely follows the height of the platelet center of mass. At larger $\dot{\gamma}$, the hydrodynamic drag flattens the platelet onto the surface, decreasing the average distance between the wall and the platelet center of mass until geometry limits further flattening. At this point, the drag force is linearly related to the shear rate, which leads to the linear relationship between translocation distance and shear rate.

4.5 Sensitivity Analysis

The fluid mechanics in our system is relatively well established. Most unactivated platelets are similar in size and shape. Zhao et al. extensively investigated the three dimensional dynamics of RBC's and demonstrated that shear flow is a good approximation to the flow field in the near wall region. On the other hand, the biological parameters in the model can change drastically across the human population. For example, a platelet in a patient suffering from a bleeding disorder

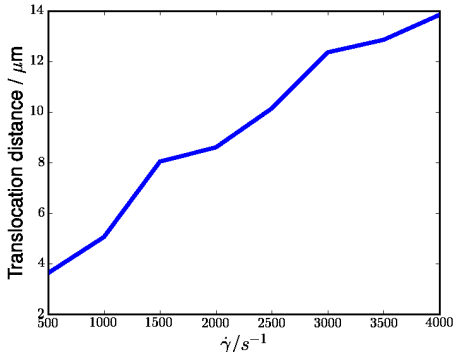

Fig. 16 Mean translocation distance for varying shear rates.

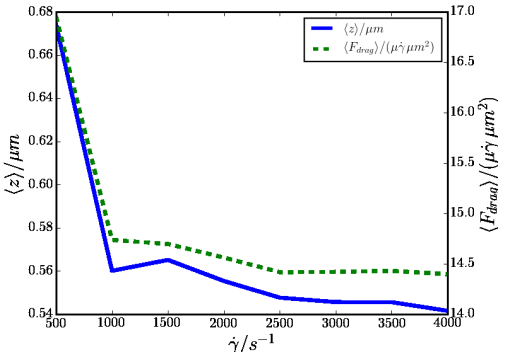

Fig. 17 Mean platelet drag force and center of mass height as a function of shear rate.

would be much less prone to adsorption than a platelet in a healthy human, which could manifest as a significantly lower $k_{\text{on}}^{\text{weak}}$. To account for variation in the population, we investigate the effects of varying microstructural parameters on observables. This subsection shows that platelet function can be indirectly inferred from experimentally observable quantities, which shows that the experiments have diagnostic relevance.

In all simulations in this section, we begin with a platelet tethered to the wall with a single weak bond (one that has just entered the transiently adhered state), and we allow the system to evolve with time. The outputs are the translocation distances and the fraction of platelets that firmly adhere. The variation of binding fraction with forward reaction rates was previously shown in Figures 13 and 14 when establishing the forward reaction parameters, $k_{\text{on}}^{\text{weak}}$ and $k_{\text{on}}^{\text{strong}}$.

In the first set of simulations, we vary $k_{\text{on}}^{\text{weak}}$, which corresponds to VWF-GPIb bond formation. The results are shown in Figures 13 and 18. The translocation distance is a strong function of $k_{\text{on}}^{\text{weak}}$ only for lower values of the reaction rate, quickly approaching an asymptote as most of the platelets adhere firmly.

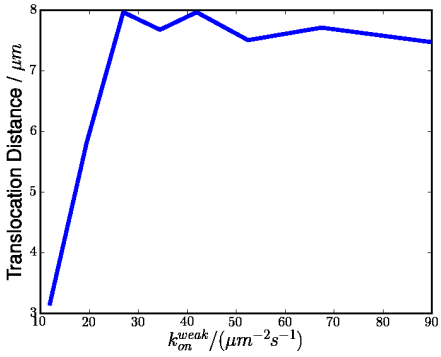

Fig. 18 Mean translocation distance vs GPIb-VWF bond formation rate.

The next simulation set, shown in Figures 14 and 19, is similar to the previous experiment, but the strong bond (spring) rate constant, $k_{\text{on}}^{\text{strong}}$, is varied. These bonds correspond to the $\alpha_{\text{IIb}}\beta_3$ bonds. In this case, increasing $k_{\text{on}}^{\text{strong}}$ reduces the translocation time before the platelet firmly adheres, slightly increasing the binding fraction while significantly reducing the translocation distance.

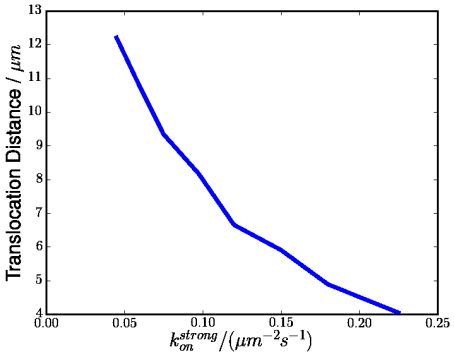

Fig. 19 Mean translocation distance vs $\alpha_{\text{IIb}}\beta_3$ bond formation rate.

The final parameter varied is L, which represents the size of the VWF molecules. The results are shown in Figures 20 and 21. L combines the effects of both $k_{\text{on}}^{\text{weak}}$ and $k_{\text{on}}^{\text{strong}}$. As L increases, more platelet area is exposed to the wall surface, so the effective bond formation rates for both bond types increase simultaneously. The mean translocation distance is controlled by weak bond formation for smaller L, and strong bond formation at larger L. The fraction of bound platelets increases monotonically as both effective reaction rates are increased.

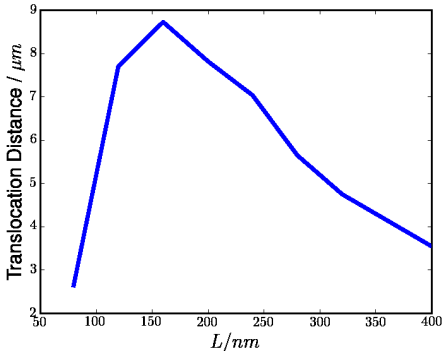

Fig. 20 Mean translocation distance vs maximum bond formation length.

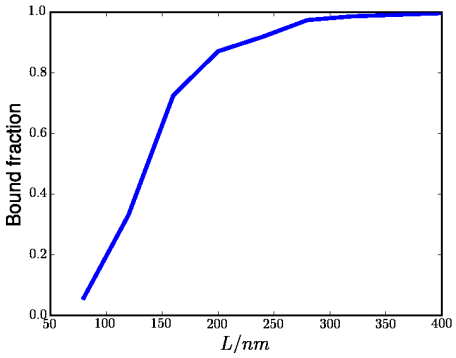

Fig. 21 Binding fraction vs maximum bond formation length.

5 State Dynamics Recap

There are four possible states for a platelet. It can found in the bulk (1), in the F-L layer (2), transiently adhered to a vessel wall (3), or firmly adhered (4). Using our simulations and comparing with experiments, we simulated the rate constants to and from the transiently adherent state, with corresponding rate constants r_{23}, r_{32}, and r_{34}. More importantly, we established the physical mechanisms which govern these parameters (Figure 2). As stated in subsection 4.1, the platelet transition rate from the F-L layer back into the core is much slower than r_{12} and can be approximated as vanishing. The transition rate r_{12} can be estimated using the margination length scale reported by Zhao et al.[3], which takes into account the flow geometry by incorporating the distance that a platelet must travel from the vessel center to the periphery. The margination length is converted into a time scale using the average channel velocity. The dispersion time scales are 6 seconds and 2 seconds respectively for $Ht = 0.1$ and $Ht = 0.2$, and the rate constants are approximated by inverting these time scales.

The estimated range for r_{23} corresponds to margination rates for hematocrit in the range of 0.1 to 0.2. There is a slight complication in interpreting the r_{32} and r_{34} values directly, since platelets entering state 3 (transient adhesion) quickly differentiate into two subsets: those that eventually firmly adhere and those that reenter the flow. Thus, although the two rate constants are comparable, most platelets that adhere transiently on a VWF-covered vessel wall eventually firmly adhere, with a probability of 0.85. Note that the rate constants from states 2 and 3 are independent of flow geometry as long as the vessel wall is approximately flat over the size of a platelet. For example, a circular tube is locally flat if the tube radius is much larger than a platelet diameter (2 microns).

All of these rate constants are on the order of $0.2s^{-1}$, which means that RBC collisions and receptor dynamics are equally important in determing the overall platelet adhesion rate.

These rate constants can be used to understand the platelet distribution in the experiments, but care must be taken when extending the model. First, the flow geometry will alter the rate of platelet margination to the near wall region, which can be quickly estimated using the theory of Zhao et al. [3] The rate of platelet diffusion back into the vessel core, r_{21}, will remain negligible in most cases, and the rate of platelet release after transient adhesion r_{32} will likewise remain constant. Unfortunately, both types of platelet adsorption are heavily dependent on the ligand-receptor bonds, so r_{23} and r_{34} must be remeasured before applying our theory to new situations. For example, patients with certain types of Von Willebrand Disease are expected to show very different platelet-wall reactivity, resulting in altered overall rate constants. Furthermore, the experimental distribution and activity of wall-bound VWF differs from the *in vivo* environment.

Table 2 Rate constant estimates

Rate	Transition	Controlling physics	Estimate
r_{12}	Bulk	Hematocrit	0.2 - 0.5s^{-1}
	$\rightarrow$ Near Wall	Weak Brownian Motion	
r_{21}	Near Wall	Hematocrit	0s^{-1}
	$\rightarrow$ Bulk	Weak Brownian Motion	
r_{23}	Near Wall	FL layer size	0.07 - 0.4s^{-1}
	$\rightarrow$ Transient adhesion	Shear flow	
		VWF-GPIb dynamics	
r_{32}	Transient adhesion	VWF-GPIb and $\alpha_{IIb}\beta_3$	0.2s^{-1}
	$\rightarrow$ Near Wall	bond dynamics	
r_{34}	Transient adhesion	VWF-GPIb and $\alpha_{IIb}\beta_3$	0.2s^{-1}
	$\rightarrow$ Firm adhesion	dynamics	

6 Conclusions

We have presented a multi-scale model for platelet adhesion in terms of a Markov process. Using Stokes flow simulations, the

transition coefficients, r_{ij} are related to various physical processes. RBC collisions push platelets out of the channel core. Further RBC collisions are then critical in driving platelets across the Fahreus-Lindqvist layer. Transient platelet adhesion is governed by shear flow and GPIb-VWF rate kinetics, while firm adhesion is mediated by $\alpha_{IIb}\beta_3$ rate kinetics. Bond formation rates were estimated from microfluidic experiments with VWF covered surfaces, and we predicted relationships between the receptor dynamics and experimental observables. Overall, we have found that RBC collisions and receptor dynamics are equally important in determining initial platelet adhesion, and our experiments can be used to diagnose altered platelet function.

Acknowledgments

We thank the US Army High Performance Computing Research Center (AHPCRC) for supporting this work. A large portion of the computer simulation was performed on the Stanford Univerity's Certainty computer cluster, which is funded by the American Recovery and Reinvestmant Act of 2009 (ARRC).

References

[1] Heu Ni and John Freedman. "Platelets in hemostasis and thrombosis: role of integrins and their ligands". In: *Transfusion and Apherisis Science* 28 (2003), pp. 257–264.

[2] C. Robert Valeri et al. "Anemia-induced increase in the bleeding time implications for treatment of nonsurgical blood loss". In: *Transfusion* 41 (2001), pp. 977–983.

[3] Hong Zhao, Eric S. G. Shaqfeh, and Vivek Narsimhan. "Shear-induced particle migration and margination in a cellular suspension". In: *Physics of Fluids* 24 (2012), p. 011902.

[4] H. Lankhof et al. "A3 domain is essential for interactino of von Willeblrand factor with collagen type III". In: *Thromb. Haemost.* 75 (1996), pp. 950–958.

[5] Kenji Nishio. "Binding of platelet glycoprotein Ib alpha to von Willebrand factor domain A1 stimulates the cleavage of the adjacent domain A2 by ADAMTS13". In: *Proc Natl Acad Sci USA* 101 (2004), pp. 10576–10583.

[6] Hans Ulrichts et al. "Shileding of the a1 domain by the D'D3 domains of von Willebrand factor modulates its interaction with platelet glycoprotein Ib-IX-V". In: *J. Biol. Chem* 281 (2006), pp. 4699–4707.

[7] Kenneth J. Clemetson and Jeannine M. Clemetson. "Platelet collagen receptors". In: *Throm Haemost* 86 (2001), pp. 189–197.

[8] Armin J. Reininger. "VWF attributes - impact on thrombus formation". In: *Thrombosis Research* 122 (2008), S9–S13.

[9] R. Anand Kumar et al. "Kinetics of GPIba-VWF-A1 tether bond under flow: effect of GPIba mutations on the association and dissociation rates". In: *Biophys Journal* 85 (2003), pp. 4099–4109.

[10] Yang Shen et al. "Functional analysis of the C-terminal flanking sequence of platelet glycoprotein Ib alpha using canine-human chimeras". In: *blood* 99 (2002), pp. 145–150.

[11] Brian Savage, Sanford J. Shattil, and Zaverio M. Ruggeri. "Modulation of platelet function through adhesion receptors: a dual forle for glycoprotein IIb-IIIa mediated by fibrinogen and glycoprotein Ib - von Willebrand factor". In: *J. Bio Chem* 267 (1992), pp. 11300–11306.

[12] A.JU. Goldman, R. G. Cox, and H. Brenner. "Slow viscous motion of a sphere parallel to a plane wall - II Couette flow". In: *Chemical Engineering Science* 22 (1967), pp. 653–660.

[13] M. Chaoui and F. Feuillebois. "Creeping flow around a sphere in shear flow close to a wall". In: *Q. App Math* 56 (2003), pp. 381–410.

[14] George I. Bell. "Models for the specific adhesion of cells to cells: A theoretical framework for adhesion mediated by reversible bonds between cell surface molecules". In: *Science* 200 (1978), pp. 618–627.

[15] George I. Bell. "Estimate of the sticking probability for cells in uniform shear flow with adhesion caused by specific bonds". In: *Cell Biophysics* 3 (1981), pp. 289–304.

[16] Daniel A. Hammer and Douglas A. Lauffenburger. "A dynamical model for receptor mediated cell adhesion to surfaces". In: *Biophys J.* 52 (1987), pp. 475–487.

[17] Cindy Cozens-Roberts, D.A. Lauffenburger, and John A. Quinn. "Receptor-mediated cell attachment and detachment kinetics". In: *Biophys J.* 58 (1990), pp. 841–856.

[18] Daniel A. Hammer and Sachin M. Apte. "Simulation of cell rolling and adhesion on surfaces in shear flow: general results and analyhsis of selectin mediated neutrophil adhesion". In: *Biophys J.* 63 (1992), pp. 35–57.

[19] Kai-Chien Chang, David F. J. Tees, and Daniel A. Hammer. "The state diagram for cell adhesion under flow: Leukocyte rolling and firm adhesion". In: *Proceedings of the National Academy of Sciences* 97 (2000), pp. 11262–11267.

[20] Chenghai Sun, Cristiano Migliorini, and Lance L. Munn. "Red blood cells initiate leukocyte rolling in postcapillary expansions: a lattice Boltzmann analysis". In: *Biophys J.* 85 (2003), pp. 208–222.

[21] Sameer Jadhav, Charles D. Eggleton, and Konstantinos Konstantopoulos. "a 3-D computational model predicts that cell deformation affects selectin mediated leukocyte rolling". In: *Biophys J.* 88 (2005), pp. 96–104.

[22] M.G. blyth and C. Pozrikidis. "Adhesion of a blood platelet to injured tissue". In: *Engineering Analysis with boundary elements* 33 (2009), pp. 695–703.

[23] Nipa A. Mody and Michael R. King. "Platelet adhesive dynamics. Part 1: characterization of platelet hydrodynamic collisions and wall effects". In: *Biophys J.* 95 (2008), pp. 2530–2555.

[24] Weiwei Wang, Nipa A. Mody, and Michael R. King. "Multiscale model of platelet adhesion and thrombus growth". In: *Annals of Biomedical Engineering* 40 (2013), pp. 2345–2354.

[25] Weiwei Wang, Nipa A. Mody, and Michael R. King. "Multiscale model of platelet translocation and collision". In: *J. Computational Physics* 244 (2012), pp. 223–235.

[26] Sangho Kim et al. "Temporal and spatial variations of cell-free layer width in arterioles". In: *Am J. Physiol. Heart Circ. Physiol.* 293 (2007), H1526–H1535j.

[27] Armin J. Reininger et al. "Mechanism of platelet adhesion to von Willebrand factor and microparticle formation under high shear stress". In: *Blood* 207 (2006), pp. 3537–3545.

[28] Brian Savage, Jan J. Sixma, and Zaverio M. Ruggeri. "Functional self association of von Willebrand factor during platelet adhesion under flow". In: *PNAS* 99 (2002), pp. 425–430.

[29] Alexander E. Moskalensky et al. "Accurate measurement of volume and shape of resting and activated blood platelets from light scattering". In: *J. Biomed Optics* 18 (2013), p. 017001.

[30] Teresa A. Doggett et al. "Alterations in the intrinsic properties of the GPIb alpha - VWF tether bond define the kinetics of the platelet type von Willebrand disease mutations, G233V". In: *Blood* 102 (2003), pp. 152–160.

[31] Kannayakanahalli M. Dayananda et al. "Von Willebrand factor self association on platelet GPIb-alpha under hydrodynamic shear: effect on shear-induced platelet activation". In: *Blood* 116 (2010), pp. 3990–3998.

[32] Klaus Bonazza et al. "Visualization of a portein-protein interaction at a single-molecule level by atomic force microscopy". In: *Analytical and Bioanalytical Chemistry* 406 (2013), pp. 1411–1421.

[33] Walter Huber et al. "Determination of kinetic constants for the interaction between the platelet glycoprotein IIb-IIIa and fibrinogen by means of surface plasmon resonance". In: *Eur. J. Biochem.* 227 (1995), pp. 647–656.

[34] Bryan Lincoln et al. "Integrated system investigating shear-mediated platelet interactions with von Willebrand factor using microliters of whole blood". In: *Analytical Biochemistry* 405 (2010), pp. 174–183.

[35] Sacha M. Dopheide, Mhairi J. Maxwell, and Shaun P. Jackson. "Shear dependent tether formation during platelet translocation on von Willebrand factor". In: *Blood* 99 (2002), pp. 159–167.

[36] Jean-Daniel Boissonnat and Steve Oudot. "Provably good sampling and meshing of surfaces". In: *Graphical Models* 64 (2005), pp. 405–451.

[37] Herbert Edelsbrunner and Ernst P. Mucke. "Three-dimensional alpha shapes". In: *ACM TOG* 13 (1994), pp. 43–72.

[38] Jonathan Richard Shewchuk. "Adaptive precision floating-point arithmetic and fast robust geometric predicates". In: *Discrete computational geometry* 18 (1997), pp. 305–363.

[39] G. K Youngren and A. Acrivos. "Stokes flow past a particle of arbitrary shape: a numerical method of soultion". In: *JFM* 69 (1975), pp. 377–403.

[40] Adolfo J. Banchio and John F. Brady. "Accelerated Stokesian dynamics: Brownian motion". In: *J. Chem Physics* 118 (2003), pp. 10323–10332.

[41] Gilbert Walker. "On periodicity in series of related terms". In: *Proceedings of the Royal Society of London, Ser. A* 131 (1931), pp. 518–532.

[42] C. Pozrikidis. "Orbiting motion of a freely suspended spheroid near a plane wall". In: *JFM* 541 (2005), pp. 105–114.

[43] Ya-Ping Wu et al. “Platelet thrombus formation on collagen at high shear rates is mediated by von Willebrand factor-glycoprotein Ib interaraction and inhibited by von Willebrand factor-glycoprtein IIb/IIIa interaction”. In: *Arteriosclerosis and Vascular Biology* 20 (2000), pp. 1661–1667.